POLITECNICO DI TORINO
Repository ISTITUZIONALE

On the correlation between process parameters and specific energy consumption in fused deposition modelling

(Article begins on next page)

20 April 2024

On the correlation between process parameters and specific energy consumption in Fused Deposition Modelling

Vincenzo Lunetto, Paolo C. Priarone*, Manuela Galati, Paolo Minetola

Politecnico di Torino, Department of Management and Production Engineering, Corso Duca degli Abruzzi 24, 10129 Torino, Italy

* Corresponding author (P.C. Priarone)
Email: paoloclaudio.priarone@polito.it
Ph.: (+39) 011 0907259
Fax: (+39) 011 0907299

Abstract

Additive Manufacturing (AM) techniques enable the layer-wise fabrication of complex shapes without the need for specific production tools, reducing the economic lot size to the single unit and allowing the mass customization. Besides the technological drivers pushing AM towards several industrial applications, the energy efficiency and the time/cost performance in comparison to more conventional manufacturing processes are still to be investigated. This research focuses on the Fused Deposition Modelling (FDM) process for the production of components made either of ABS or PC-ABS. The impact of the main variables (such as the layer thickness and the infill strategy) on the process time and the energy consumption was analysed while considering the FDM unit-process. Empirical predictive models correlating the energy efficiency with the main process variables are proposed in this paper. The results confirm that the Specific Energy Consumption approach already applied to other manufacturing unit-processes can be successfully extended to FDM. Moreover, the increase in the average Deposition Rate, which is related to the deposition path, appears to be a strategy for the reduction of the specific printing energy. Such experimental evidence might suggest further energy-conscious improvements in the design of AM processes and equipment.

Keywords: Sustainable manufacturing; 3D printing; Deposition rate; Energy efficiency.

1. Introduction and motivation

Additive Manufacturing (AM) processes allow the layer-by-layer fabrication of components made either of metal or plastic materials, starting from a three-dimensional CAD model and without any additional tool [1]. One of the main disruptive advantages brought to the manufacturing sector is related to the design freedom and the part complexity that can be achieved, together with the opportunity of using multi-materials with multi-functional properties [2]. Also, the re-design for AM, allowing the topological optimization of structural parts, provides significant benefits towards light-weighting [3, 4]. AM processes are applied in several industrial contexts, such as aerospace, automotive, biomedical applications, digital art, and architectural design, because of the wide variability of technological solutions [5]. The Additive Manufacturing of metal parts is under the spotlight, and the polymer-based processes have already proved to be cost-effective and competitive with respect to the conventional ones [6, 7], particularly if optimization of the process parameters is carried out to guarantee satisfactory mechanical properties [8]. Among the AM techniques to produce plastic parts, the material extrusion process patented by Stratasys as Fused Deposition Modelling (FDM) is widely used for the equipment simplicity, the low costs, and the capability to process different materials, even if nano-reinforced [9] or characterized by a high melting point (as PEEK [10]).

Two crucial issues for the additive manufacturing techniques are the high energy demand and low productivity, especially in comparison with subtractive and bulk processes [11-14]. The Specific Energy Consumption (SEC) model, introduced by Kara and Li [15, 16] when characterizing subtractive unit-processes, has proved to be applicable also to the additive manufacturing context to quantify the energy efficiency in material deposition (i.e., by assuming a unit mass of deposited material as the functional unit). Many authors focused on the determination of the SEC for the main AM technologies. In particular, wide variability in the SEC data concerning Fused Deposition Modelling (FDM) processes is available in the literature, as summarized in Table 1. Luo et al. [17] studied the FDM process when printing ABS components and compared the energy efficiency of different Stratasys machines (namely: FDM 1650, FDM 2000, FDM 8000 and FDM Quantum). The Stratasys FDM 8000 allowed the lowest SEC value and the authors demonstrated, for the first time, the correlation between the SEC value and the FDM machine architecture. The SEC data in [17] were also referenced in further researches [11, 12, 18, 19]. Mognol et al. [20] analysed the achievable reduction in the overall energy consumption of FDM by changing the orientation of the 3D-printed component inside the build chamber. The machine was a Stratasys FDM 3000, with a mean operational power of 570 W, and the printed material was ABS. The quantity of material needed for the support structures (which, in turn, depends on the part orientation) was found to be the main driver on the energy demand, whereas the height of the printed component appeared to be of secondary importance. The paper of Mognol et al. [20] was one of the first studies concerning sustainability and the energy efficiency of the FDM process and was used as a life cycle inventory source for subsequent works [11, 19, 21].

Baumers et al. [22] performed experimental trials on different AM processes and studied the influence of the build capacity utilization on the energy efficiency of the machine (and, therefore, on the SEC value). Focusing on the FDM process, a Stratasys FDM 400mc machine was used to produce parts made of polycarbonate. A slight variation in the SEC value was noticed when using the FDM machine for a single part production or at its full capacity utilization. This evidence was traced back to the low power demand of the warm-up phase and the absence of an energy-demanding cool-down phase. Under the same process configurations, the research highlighted much more significant differences in the SEC values for the metal deposition processes. The results for FDM by Baumers et al. [22] were also recalled in [11, 12, 19, 23]. Some authors [14, 19, 24] focused on the characterization of the power profile for different machines (i.e., Stratasys Dimension SST 1200 es, Stratasys Dimension SST and Makerbot Replicator 2x) and identified the contributions to the total energy demand due to the main sub-phases of the FDM process. In particular, Yosofi et al. [19] studied the correlation between the SEC parameter and the component geometry. Components with a higher Z-height were found to have a higher SEC, because of the higher build time. Yosofi et al. [25] proposed a multi-criteria evaluative approach to compare the performance of five different FDM machines (i.e., MakerBot Replicator 2x, 3D Systems RapMan 3.2, Stratasys Mojo, HP Designjet 3D and Stratasys Dimension Elite) under the technical, economic, and environmental perspective. Roughness, costs, water and energy consumption as well as the material flows were quantified. As far as the energy efficiency is concerned, the data

reported in Table 1 were further elaborated from the literature to compute the SEC factors as the ratio between the energy consumption (MJ) and the deposited mass (kg).

Table 1. SEC data available in the literature for the Fused Deposition Modelling (FDM) process.
The values marked with '*' have been computed and adapted by the authors of the present paper.

Machine	Material	Mean operational power (W)	SEC (MJ/kg)	Reference(s)
Stratasys FDM 1650	ABS	1320	1247	[11, 12 ,17-19]
Stratasys FDM 2000	ABS	2200	416	[11, 12, 17-19]
Stratasys FDM 8000	ABS	2200	83	[11, 12, 17-19]
Stratasys FDM Quantum	ABS	11000	589	[11, 12, 17-19]
Stratasys FDM 3000	ABS	570	228 - 447 *	[11, 19-21]
Stratasys FDM 400mc (Single part)	PC	2450	536	[11, 12, 19, 22, 23]
Stratasys FDM 400mc (Full build)	PC	2450	519	[11, 22, 23]
Stratasys Dimension SST 1200es	ABS	580	171 - 219	[12, 14, 19]
Stratasys Dimension 768 SST	ABS P400	1100	689	[11, 12, 19]
Stratasys Dimension SST	n.a.	1100	n.a.	[11, 24]
Makerbot Replicator 2x	ABS	125 *	28 - 47	[19]
MakerBot Replicator 2x	ABS	125 *	23 *	[19, 25]
3D Systems RapMan 3.2	ABS	n.a.	19 *	[25]
Stratasys Mojo	ABS	n.a.	40 *	[25]
HP Designjet 3D	ABS	n.a.	77 *	[25]
Stratasys Dimension Elite	ABS	n.a.	127 *	[25]

The SEC values listed in Table 1 differ by one (or even two) order of magnitude. This evidence underlines a huge variability in the energy efficiency performance of different systems and architectures of the machines (some of which are devoted to industrial use, whilst others are for a semi-professional use). Regarding the state-of-the-art literature, some knowledge gaps can be identified. First, the role of the FDM machine architecture on Specific Energy Consumption is not clearly defined. Second, the effects of (*i*) the printed material, (*ii*) the main process parameters (such as the layer thickness, the infill strategy, the position of the part on the build table), (*iii*) the geometrical complexity of the part on the process energy efficiency are still to be investigated. The paper aims to fulfil the above-listed knowledge gaps and to define a correlation between the main process variables and the energy efficiency in FDM processes. Experimental tests were designed and performed using a Stratasys F370 machine. The methodological approach and the rationale behind the chosen ranges of process parameters are detailed in Section 2. The results in terms of material flows, electric energy consumption and process time are presented in Section 3. Empirical models for the Specific Printing Energy (SPE) and the Specific Energy Consumption (SEC) of the process while varying the average Deposition Rate are proposed and discussed in Section 4. The conclusions are summarized in Section 5.

2. Materials and methods

Six components characterized by a different geometrical complexity were identified (as shown in Figure 1) while taking into account the typical features that can be industrially produced with respect to the capabilities of the FDM process. In particular, the component labelled with 'A' is a basket with a complex, thin and branched structure which is difficult to produce by means of manufacturing routes such as injection molding or machining. The components 'B' and 'C' are brackets that were re-designed for AM by using topological optimization procedures. The components 'D', 'E' and 'F' are simple and massive geometries with different surface-to-volume ratios, that could still be suitable for AM, especially for production volumes tending towards the single-part production [6]. The volume enclosed into the surfaces of the STL file and the maximum dimensions of the parallelepiped enveloping each component are listed in Table 2.
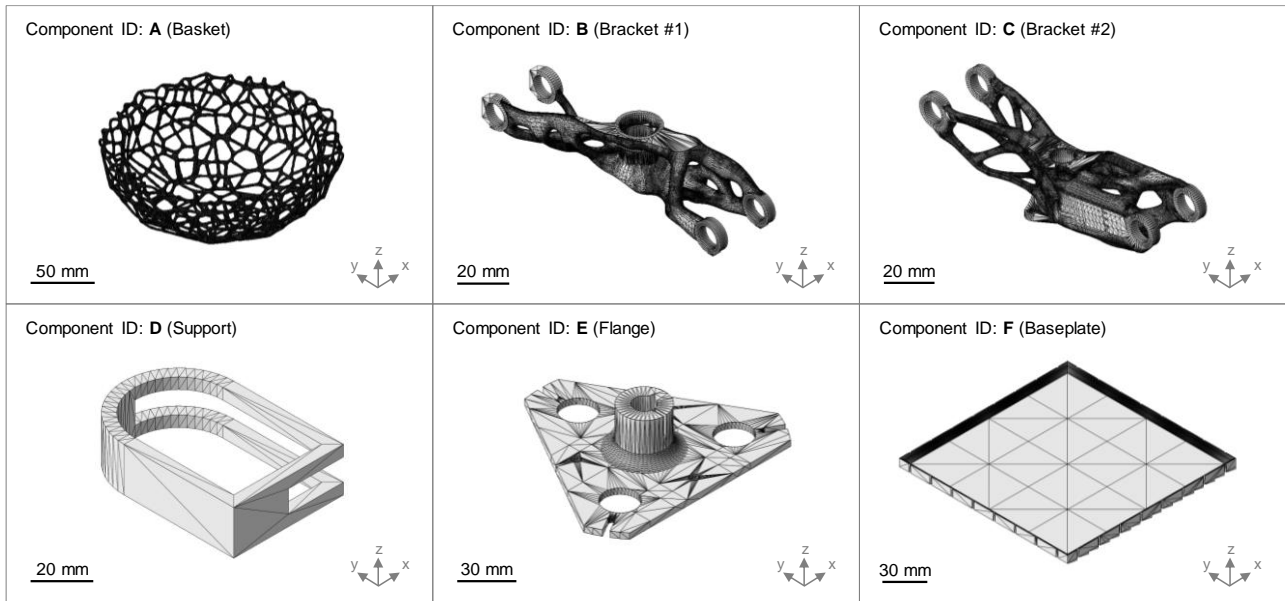

Figure 1. Selected components.

**Table 2.** Geometrical specifications for each component.

Component	ID	Component volume, STL file (mm³)	Maximum dimensions (mm × mm × mm)
Basket	A	23.34×10^3	153.9 × 155.1 × 50.7
Bracket #1	B	14.80×10^3	32.1 × 131.1 × 27.9
Bracket #2	C	19.46×10^3	41.1 × 132.3 × 29.1
Support	D	15.80×10^3	51.3 × 76.5 × 21.3
Flange	E	54.48×10^3	141.3 × 123.9 × 33.3
Baseplate	F	84.09×10^3	161.1 × 161.1 × 10.5

The components were produced in ABS or PC-ABS by means of a Stratasys F370 FDM machine (Figure 2). The support structures were built by using the Stratasys QSR proprietary material. Version 1.22 of the GrabCAD Print software by Stratasys was used to slice the STL models of the components and generate the printing paths and code. Two different layer thicknesses of 0.178 mm and 0.330 mm were selected. Once chosen, the thickness was fixed and constant for all the layers. Within the GrabCAD Print software, three different infill strategies (namely: the so-called 'solid', S, 'sparse high-density', HD, and 'sparse low-density', LD) were selected for the slicing of the parts. The 'solid' (S) strategy provides the highest density (with infill lines that touch each other) and the lowest porosity. It is generally used for structural components and implies high material consumption and long printing time. Conversely, in the 'sparse low-density' (LD) strategy, the

infill lines are widely spaced (about 2 mm) to allow for material savings and shorter printing times. The 'sparse high-density' (HD) strategy provides an intermediate result if compared to the previous ones. The infill lines are rather close (about 2 lines every millimeter), but not as much as in the solid case (Figure 3).
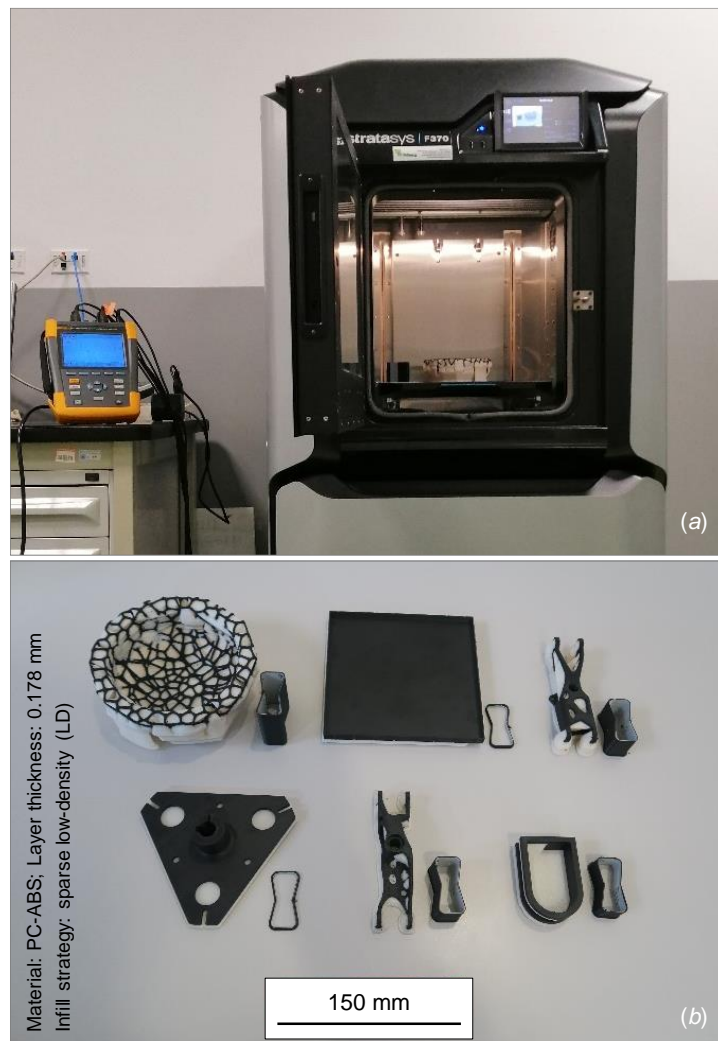
Figure 2. Experimental setup (*a*) and additively manufactured components (*b*).
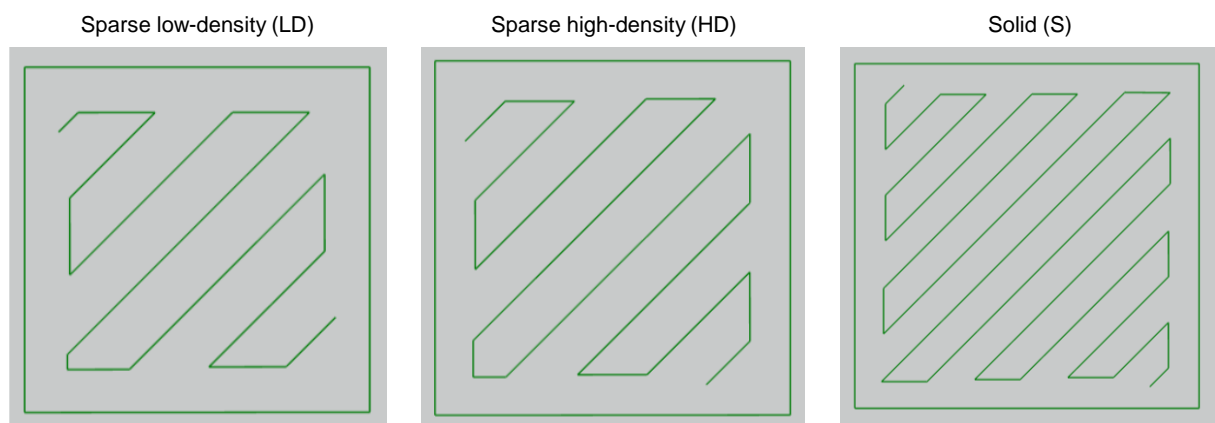
Figure 3. Different infill strategies within the GrabCAD Print software for a simple cube.

Among all the possible combinations of geometries and process parameters, a subset of experimental tests was identified to achieve a wide variation in the average Deposition Rate (which was preliminarily simulated by means of the GrabCAD Print software), with the aim of investigating its effects on Specific Energy Consumption (SEC) and Specific Printing Energy (SPE). In addition, to better highlight the correlation between the process parameters and the measured outcomes, a full factorial plan was designed for the experiments concerning the 'E' component. The (*i*) layer thickness (0.178 mm or 0.330 mm), the (*ii*) infill strategy (S, HD or LD) and the (*iii*) component material (ABS or PC-ABS) were the three considered factors. Among the other components, the Flange ('E') was chosen since the high number of layers with large areas allowed the GrabCAD Print software to significantly diversify the extrusion path while changing the process parameters. All the tests were run by setting the machine in the so-called 'eco-mode', in which the temperature of the build chamber is cooled down to the room temperature at the end of the job. The jobs were randomly located onto the build plate, and a purge part was produced in each job to guarantee the cleaning of the extruders and, hence, the quality of manufactured components and support structures. The 'last swap' option was chosen to reduce the material consumption. Under this configuration, the height of the purge part corresponds to the height of the last layer in which there is an alternate deposition of materials of which component and support structures are made of. The main process parameters and the material properties are listed in Table 3. The build chamber was heated up to 90°C and 95°C for ABS and PC-ABS, respectively. The extrusion temperature of PC-ABS was 30°C higher than that of ABS, due to the different rheological properties of each material. A slight difference in the specific gravity of PC-ABS and ABS was found in the datasheet of the build materials [26, 27]. This implied that, for a fixed volume of the produced component, slight differences were expected in the part weight. The soluble QSR material by Stratasys for support structures was extruded at 265°C during printing and kept at 170°C when the extruder was not in use. The QSR material was then dissolved by immersing the printed job in a solution of 600 g of sodium hydroxide in 40 l of water at 70°C for 8 hours.

Table 3. Process parameters and main characteristics for Stratasys ABS [26] and PC-ABS [27] materials.

Parameter	Stratasys ABSplus-P430	Stratasys PC-ABS
Chamber temperature	90°C	95°C
Extrusion temperature	255°C (Printing); 190°C (Not in use)	285°C (Printing); 190°C (Not in use)
Specific gravity (ASTM D792)	1.04	1.10
Tensile strength (ASTM D638)	33 MPa	41 MPa
Tensile modulus (ASTM D638)	2200 MPa	1900 MPa
Tensile elongation at break (ASTM D638)	8%	6%
Heat Deflection Temperature (HDT) @ 66 psi (ASTM D648)	96°C	110°C
Heat Deflection Temperature (HDT) @ 264 psi (ASTM D648)	82°C	96°C
Vicat softening temperature	Not available	112°C
Glass transition temperature	108°C	125°C
Coefficient of thermal expansion	$8.82 \cdot 10^{-5}$ mm/mm/°C	$7.38 \cdot 10^{-5}$ mm/mm/°C

2.1. Methodology

The methodology applied in the present research is schematized in Figure 4. The FDM process time was measured during each test. All the profiles of current, voltage, power and energy were acquired by using a Fluke 435 Series II analyzer. The mass of each printed job was weighted (after and before the dissolution of the QSR support material) by means of a Gibertini 1000HR-CM balance with a resolution of 0.01 g. The masses of components, support structures, and purge parts were quantified. Then, data were analyzed to compute the average Deposition Rate, the Specific Energy Consumption (SEC) and the Specific Printing Energy (SPE, that is, the SEC during the deposition phase only). The results are presented and discussed in the following while focusing on the effects of the main input variables on the process outcomes. Moreover, empirical models correlating SEC and SPE with the average Deposition Rate were proposed and validated afterwards.
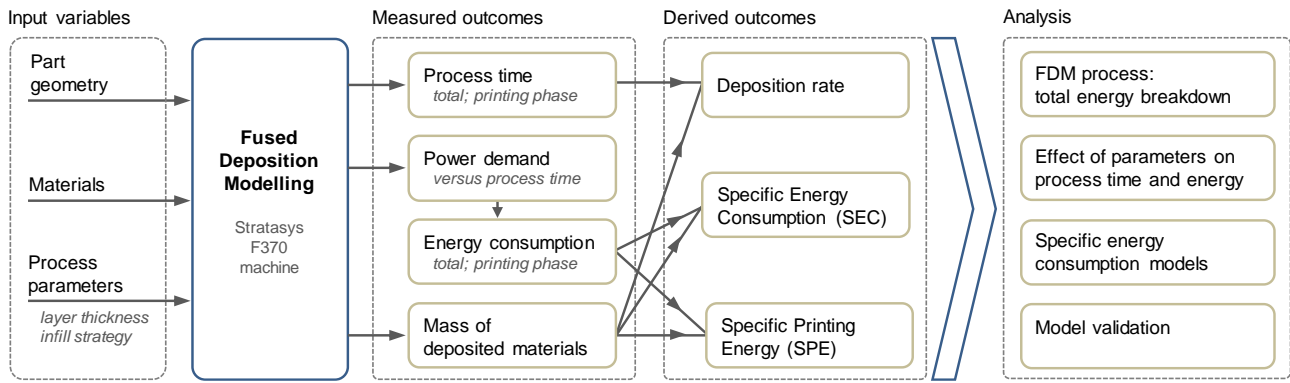
**Figure 4.** Flowchart highlighting the applied methodology.

3. Results

The experimental results regarding the electric energy consumption and the masses of the printed components are presented in the sub-sections 3.1 and 3.2, respectively.

3.1. Electric energy consumption

The power demand of the Stratasys F370 FDM machine was analyzed per each printed component in order to quantify the electric energy consumption. Figure 5 plots an example of the current profile as a function of the process time (from the switch-on of the machine until the end of the job) when additively manufacturing (in ABS) the component labelled as 'Bracket #2' in Figure 1. Some of the most significant regions of the current profile are highlighted by means of a detailed view. Five main process phases were identified: (1) switch-on; (2) idle #1; (3) heating and calibration; (4) printing; (5) idle #2. In the 'switch-on' phase ('1'), the machine is powered and goes into its stand-by mode. The variations in the current profile in Figure 5 are due to the switching on of the electronic parts as well as the initial calibration of axes and the heating system. In the 'idle #1' phase ('2') the machine is waiting for the upload of the file containing the information regarding the job (such as the build material and the extruders' path) and the command of the operator to start the 3D printing process. This phase is characterized by a constant power demand of 30 W, and its duration hinges on the operator. In the 'heating and calibration' phase ('3') the machine heats the chamber up to the process temperature, which in turn depends on the kind of material being printed. The power demand is almost constant during the entire phase. However, once the temperature of the build chamber is close to the target one for the given material, the heating system is powered by using a duty cycle. In addition, at the same time, the calibration of the axes (for extruders and table jog) starts, together with the heating of the extruders to the printing temperature. In the 'printing' phase ('4') the component and its support structures are deposited. The first layers are used to create the base to attach the build to the table of the machine. In this earlier sub-phase, the heating system of the chamber is continuously powered. The phase '4' is characterized by a typical duty cycle, as detailed in Figure 5, and the energy consumption is mainly due to the chamber heating. The duration of the printing phase depends on the dimensions and on the complexity of the job. The 'idle #2' ('5') phase starts when the last layer of the build is completed. Then, the build chamber is kept at the process temperature, until the machine receives a command from the operator who confirms that the job is removed from the table. After that command, the machine returns into its stand-by mode. The differences in maximum and minimum values of the duty cycles of phase '4' and phase '5', which are highlighted by a detailed view in Figure 5, also allow quantifying the contribution to the total power demand due to the heating of the extruders, the axes jog and the wire supply feeders. Such a contribution is proved to be small in comparison to the one of the chamber heating system.

Component: C (Bracket #2); Material: ABS; Layer thickness: 0.178 mm; Infill strategy: Sparse low-density (LD)
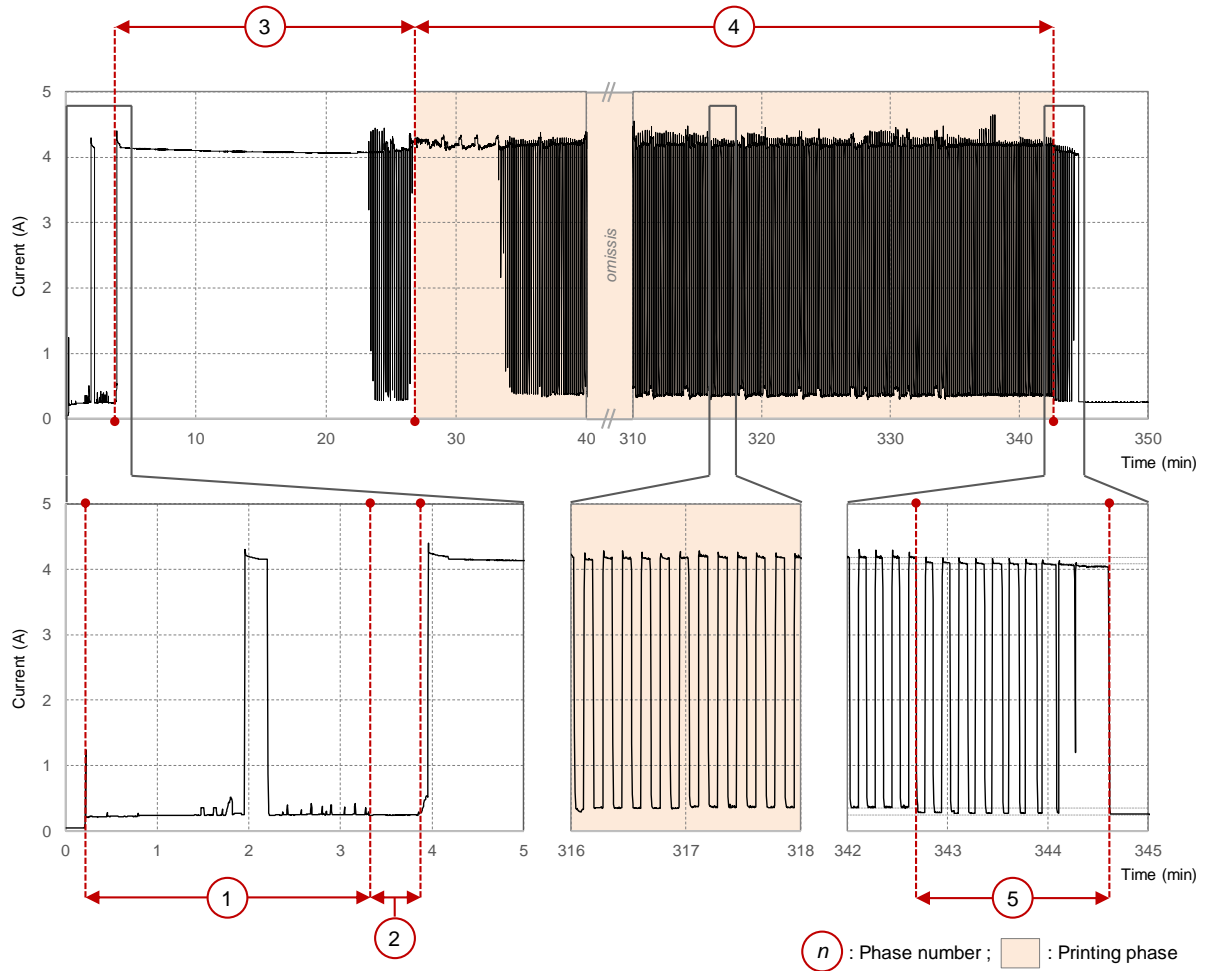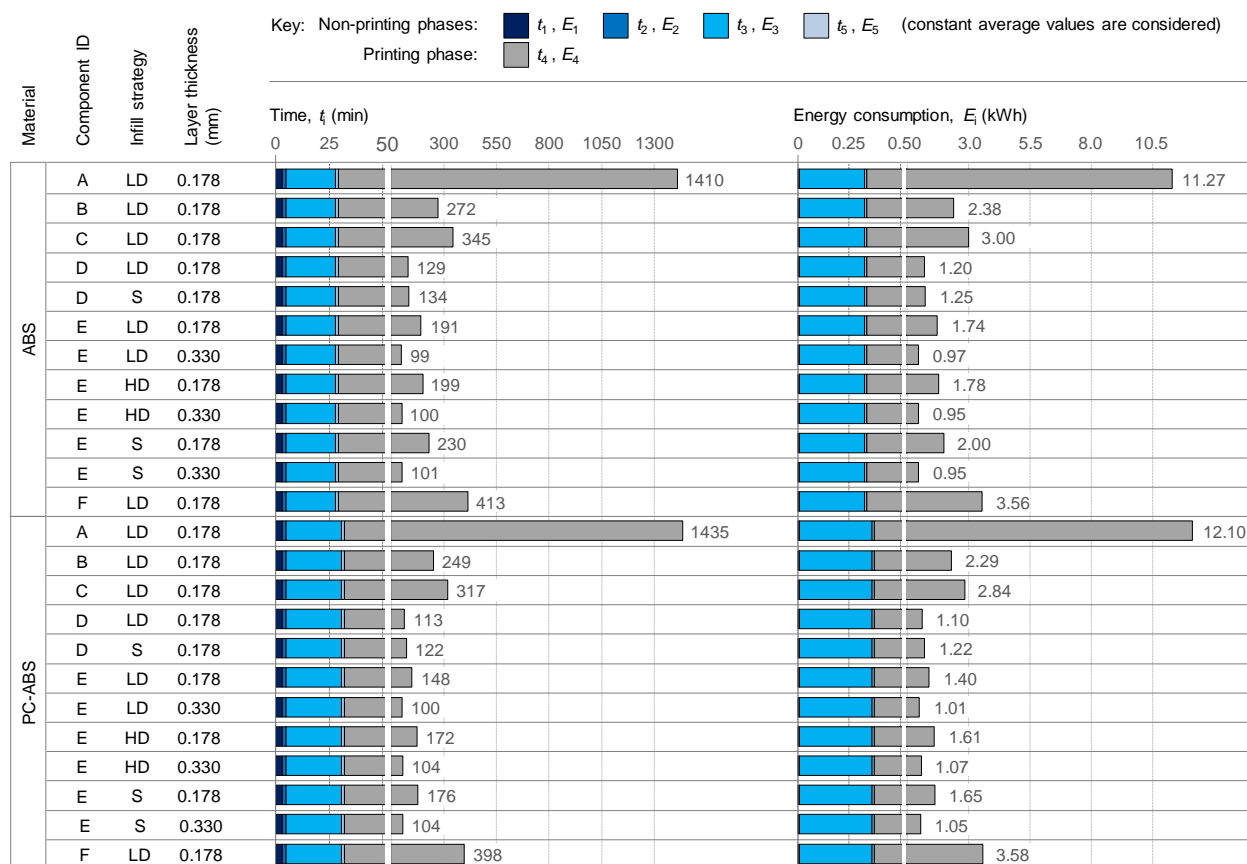
Figure 5. Data acquisition and identification of the main process phases.

Table 4. Contributions to process time and electric energy consumption due to the non-printing phases.

Phase	Process time (min)		Energy consumption (Wh)	
	Average	Range	Average	Range
(1) switch-on	3.2	[3.1 - 3.6]	5.4	[5.2 - 5.6]
(2) idle #1	1.5	[1.0 - 2.0]	0.9	[0.6 - 1.2]
(3) heating and calibration	ABS: 23.0 PC-ABS: 25.8	ABS: [20.9 - 24.4] PC-ABS: [25.2 – 26.6]	ABS: 319.1 PC-ABS: 356.3	ABS: [287.8 - 340.2] PC-ABS: [349.5 - 370.9]
(5) idle #2	1.5	[1.0-2.0]	11.9	[7.9 - 15.9]

The process time and the electric energy consumption were quantified per each job and each process phase. The only phase which is dependent on the component being manufactured is the 'printing' phase ('4'). The contributions due to the phases labelled in Figure 5 with the numbers '1', '2', '3' and '5' can be assumed to be constant. The duration and the energy demand of the 'heating and calibration' phase ('3') are a function of the printed material (i.e., ABS or PC-ABS), because of the differences in the operating temperature of the build chamber (as detailed in Table 3). Moreover, the phases '2' and '5' rely on the operator, who has to provide the FDM machine a manual command to proceed. In the present research, a constant time of 1.5 (± 0.5) min was considered for both these phases, on the basis of the experimental evidence. The average contributions of the non-printing phases are listed in Table 4, together with the minimum-maximum ranges, including all the experimental measurements. The total process time and the electric energy consumption results for all the experimental tests are summarized in Figure 6.

Figure 6. Process time (*left*) and energy consumption (*right*) results.

Key: Non-printing phases: t_1, E_1; t_2, E_2; t_3, E_3; t_5, E_5 (constant average values are considered). Printing phase: t_4, E_4.

Material	Component ID	Infill strategy	Layer thickness (mm)	Time, t_i (min)	Energy consumption, E_i (kWh)
ABS	A	LD	0.178	1410	11.27
ABS	B	LD	0.178	272	2.38
ABS	C	LD	0.178	345	3.00
ABS	D	LD	0.178	129	1.20
ABS	D	S	0.178	134	1.25
ABS	E	LD	0.178	191	1.74
ABS	E	LD	0.330	99	0.97
ABS	E	HD	0.178	199	1.78
ABS	E	HD	0.330	100	0.95
ABS	E	S	0.178	230	2.00
ABS	E	S	0.330	101	0.95
ABS	F	LD	0.178	413	3.56
PC-ABS	A	LD	0.178	1435	12.10
PC-ABS	B	LD	0.178	249	2.29
PC-ABS	C	LD	0.178	317	2.84
PC-ABS	D	LD	0.178	113	1.10
PC-ABS	D	S	0.178	122	1.22
PC-ABS	E	LD	0.178	148	1.40
PC-ABS	E	LD	0.330	100	1.01
PC-ABS	E	HD	0.178	172	1.61
PC-ABS	E	HD	0.330	104	1.07
PC-ABS	E	S	0.178	176	1.65
PC-ABS	E	S	0.330	104	1.05
PC-ABS	F	LD	0.178	398	3.58

3.2. Masses

The measured masses of each produced job are reported in Figure 7. The results are presented by separating the contributions of the component material and the QSR material to the total mass, including the amount due to the purge part. It might be noticed that the mass of the support structures (*i*) does not vary while changing the deposited material (i.e., ABS or PC-ABS) or the infill strategy (i.e., S, HD or LD); (*ii*) is affected by the layer thickness; (*iii*) increases while increasing the geometrical complexity of the component and its plan projection. As a matter of fact, the component 'A' requires structures to support the branched geometry for more than 80% of the total job weight, whereas the component 'F', despite its reduced complexity, needs a significant amount of support material (higher than 40% of the total weight) to create the large base. The masses of the ABS components are not always lower than those of the PC-ABS ones (as shown in Figure 7), even when adopting the same infill strategy and layer thickness to produce the same geometry. Such differences can be traced back to the deposition path of the extruders. For the sake of clarity, Figure 8 compares (for both the ABS or PC-ABS materials) some deposition paths for the component 'B'. The deposition paths for the QSR material (drawn in yellow color) do not change while varying the process parameters. Conversely, once the (LD, HD or S) infill strategy is chosen, the GrabCAD Print software computes, for the same layer, different paths for ABS or PC-ABS (drawn in green color). Such a difference is much more evident for the 'LD' infill strategy, while the extruders' paths become comparable when a denser infill strategy is selected. As far as the results for the component 'E' are concerned: (*i*) when the 'S' infill strategy is adopted, the mass of the PC-ABS part is higher than that of the ABS one, for both the layer thicknesses, according to the slight differences in the specific material densities; (*ii*) when the 'LD' infill strategy is implemented, the mass of the ABS parts is higher for both the layer thicknesses, due to the tightened deposition path elaborated by the software of the machine. Overall, the final mass of a printed component depends on the extruders' paths, which in turn are influenced by the layer thickness, infill strategy and kind of deposited material.

Figure 7. Masses of the printed materials per each job.

Figure 8. Infill strategies as a function of the component material.

4. Discussion

The assessment of energy consumption and resource efficiency in manufacturing can be performed at different system levels [28]. Focusing on the unit-process level, the modelling methods are usually classified into black-box approaches and bottom-up approaches. The former correlate the input process parameters empirically with an output, such as the energy consumption of the machine. The latter fractionate the output into the contributions due to the machine states or components [29]. In this section, the contributions to the total electric energy demand of the FDM machine are discussed, and empirical models are proposed.

4.1. Energy demand of FDM

The electric energy consumption and the total process time (Figure 6), can be obtained by adding the contributions of the printing phase to those of the non-printing phases. As above mentioned, the phases labelled in Section 3.1 with the numbers '1', '2', '3' and '5' are not related with the component geometry, the process parameters or the deposited material (with the sole exception of the phase '3', in which the measured differences can be traced back to the different temperatures of the build chamber when printing ABS instead of PC-ABS). Their contributions, even if affected by a limited experimental variability, can be modelled as a constant, for a given material to be deposited (according to Figure 6). Vice versa, the contribution due to the printing phase (labelled with the number '4') varies while changing the component being printed as well as the process parameters. All the experimental results highlight a linear correlation between the energy demand for the printing phase (E_4, in MJ) and the build time (t_4, in min), as shown in Figure 9. As a matter of fact, the acquired profile of the power demand versus the printing time for the Stratasys F370 machine shows a typical duty cycle (as displayed by the current profile plotted in Figure 5), which can be approximated by means of constant average power demand. Therefore, the higher the printing time is, the higher the energy consumption.
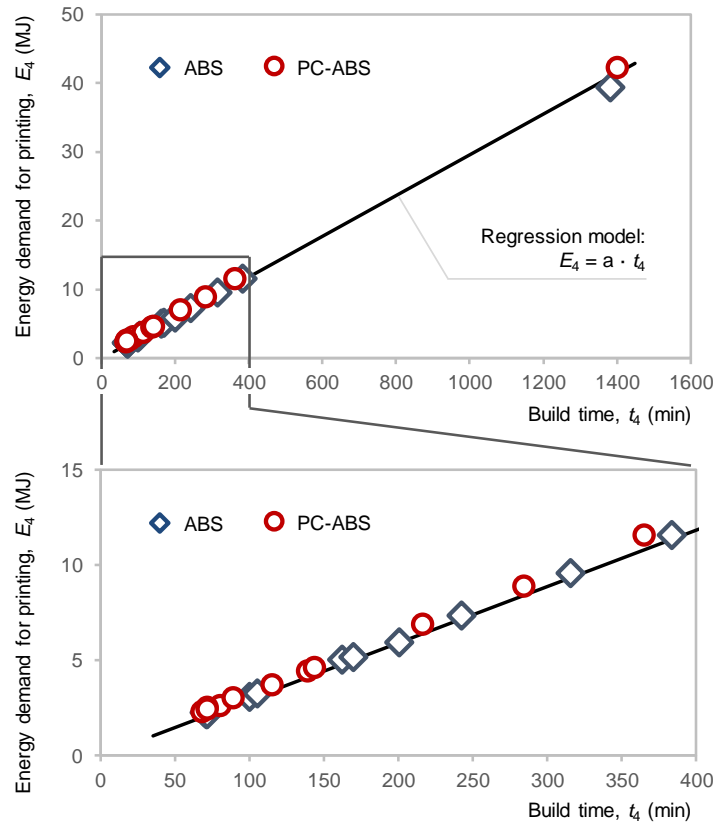

Figure 9. Correlation between the energy demand for printing (E_4) and build time (t_4).

Overall, the total electric energy consumption of the FDM process (E^{FDM}, in MJ) can be computed by summing all the i-th constant and variable contributions of each phase, according to Equation 1. The values of the 'a' coefficient were calculated by means of MATLAB R2019a software, and are listed in Table 5. The 'a' value when printing the PC-ABS material is slightly higher than that for ABS, and this is due to the different extrusion temperatures (declared in Table 3).

$$E^{\mathrm{FDM}} = \sum_{i=1}^{5} E_i = E_{\mathrm{constant}} + E_4 = E_{\mathrm{constant}} + a \cdot t_4 \tag{1}$$

Table 5. Values of the 'a' coefficient. The regression model is E_4 (MJ) = $a \cdot t_4$ (min).

Set of data	a (MJ/min)	[95% confidence bounds]	R^2
Components printed in ABS	$2.89 \cdot 10^{-2}$	[$2.84 \cdot 10^{-2}$, $2.94 \cdot 10^{-2}$]	0.99
Components printed in PC-ABS	$3.03 \cdot 10^{-2}$	[$2.99 \cdot 10^{-2}$, $3.07 \cdot 10^{-2}$]	0.99
All the printed components	$2.96 \cdot 10^{-2}$	[$2.92 \cdot 10^{-2}$, $3.00 \cdot 10^{-2}$]	0.99

4.2. Effects of process parameters on energy consumption

This section analyses the influence of process parameters (such as the layer thickness, the infill strategy and the kind of deposited material) on the achieved results for the component 'E' (i.e., the flange). Figure 10 shows graphically the main effects of the process parameters on the printing energy (black lines) and time (green lines). All the investigated levels of process parameters affect the response in terms of time and energy. The steeper slope for the layer thickness compared to the infill strategy and material indicates a greater effect. As expected, the energy demand for the printing phase (E_4) and the time (t_4) significantly decrease when the layer thickness increases from 0.178 mm to 0.330 mm. A thinner layer thickness means a greater number of layers to be deposited. Therefore, as the number of layers increases, the total length of the extruder path increases; consequently, the time for the printing phase (t_4) increases, together with the related energy consumption. On the other hand, the total length path also depends on the infill strategy. LD corresponds to a shorter path, therefore, lower energy and time are required for the printing. The analysis of material effect confirms that the machine software differently manages the two materials (as shown in Figure 8).
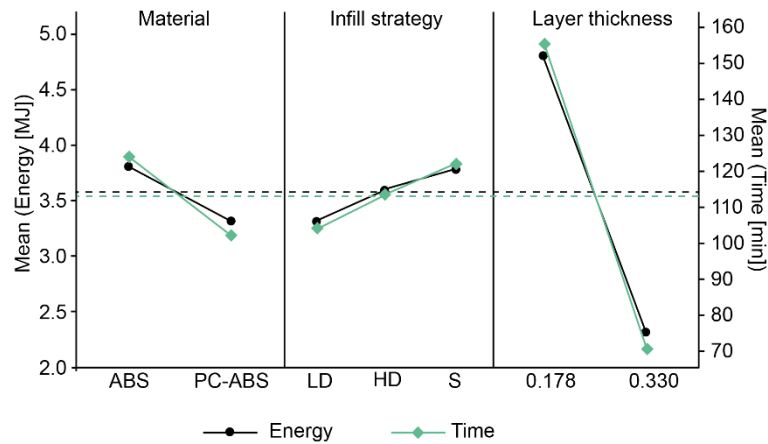
Figure 10. Main effect plot for the energy demand for printing and the build time.

Similar considerations can be drawn by analyzing the variation of energy and time as a function of the total mass of the deposited materials, including component, support structures, and purged filaments (Figure 11). As far as the power demand when printing is concerned, negligible differences can be noticed when the extruder is depositing the material of the component or the QSR material of the support structures. Therefore, the total deposited mass (m_{tot}) is considered in the following discussion. As previously noticed, for fixed layer thickness, the process time and the energy demand increase when a denser infill strategy is chosen (i.e., when shifting from a 'low density' to a 'solid dense' component). Such

differences are less significant for the layer thickness of 0.330 mm, as the number of layers decreases. A reduction in time and energy demand for the components made of PC-ABS can be noticed for a layer thickness of 0.178 mm, despite the higher process temperatures which are requested by the material (Table 3), while the results for a lower number of layers (i.e., for a layer thickness of 0.330 mm) are comparable.
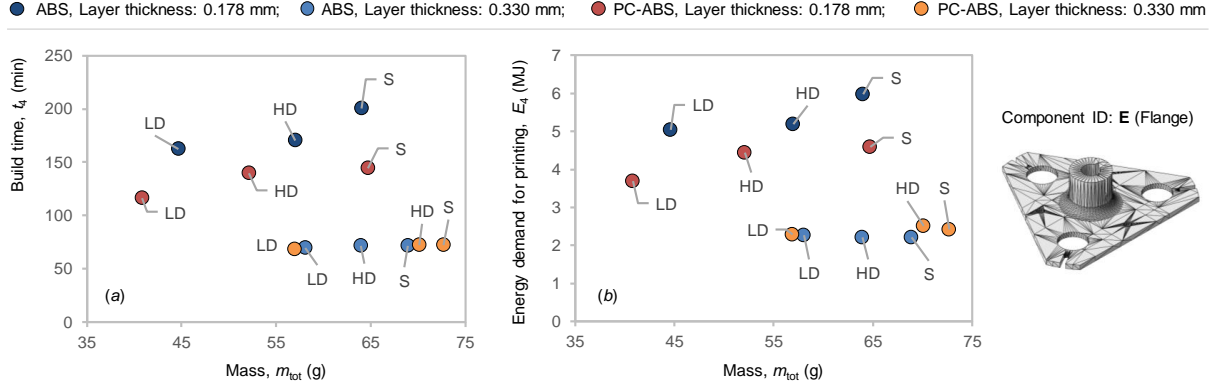
Figure 11. Effect of process parameters on build time (*a*) and energy demand for printing (*b*).

4.3. Empirical models for energy consumption

As far as the printing phase (previously labelled with the number '4') is considered, a Specific Printing Energy (SPE, in MJ/kg) can be defined, for the purposes of the present research, as the ratio between the electric energy consumption for printing (E_4, in MJ) and the total mass of the deposited materials (m_{tot}, in kg, which includes the masses of component, support structures and purge part). Moreover, an average Deposition Rate (DR_a, in kg/min) can be quantified as the ratio between m_{tot} (in kg) and the printing time (t_4, in min). All the experimental results showing the correlation between the so-defined variables are plotted in Figure 12.
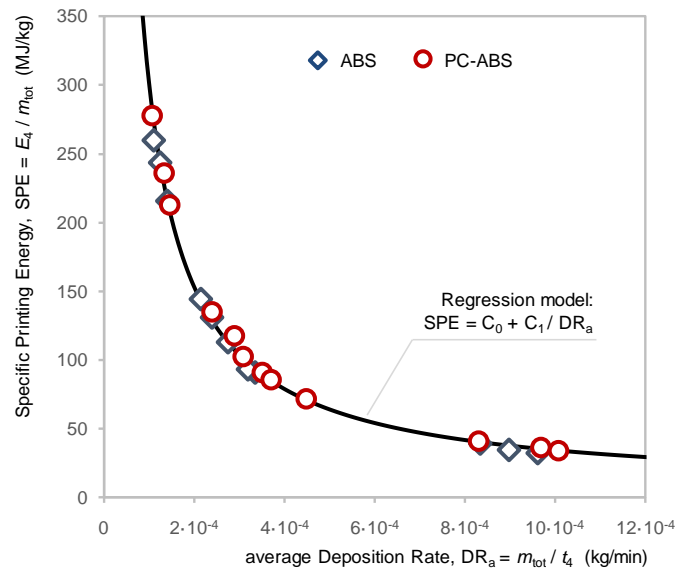
Figure 12. Specific Printing Energy (SPE) versus average Deposition Rate (DR_a).

The SPE values decrease when the DR_a increases. The here-defined average Deposition Rate (DR_a) can be seen as a proxy of the efficiency in material deposition relative to the build time. For a given mass of material to be deposited, the higher the DR_a is, the lower the deposition time. The DR_a for the Stratasys F370 FDM machine represents a holistic measure of the complexity of the deposition path, which in turn depends on the chosen process parameters, the material

to be deposited and the component shape. In fact, with respect to the results concerning the component 'E' (i.e., the flange), the DR_a has experimentally proved to increase (*i*) when increasing the layer thickness, (*ii*) when choosing an infill strategy towards a 'solid dense' part, (*iii*) when using PC-ABS instead of ABS. An analysis performed by means of MATLAB R2019a software revealed that a hyperbolic curve provides the best fit of the results plotted in Figure 12, according to the empirical model proposed in Equation 2.

$$\text{SPE} = C_0 + \frac{C_1}{\text{DR}_a} \tag{2}$$

Table 6. Values of the 'C_0' and 'C_1' coefficients. The regression model is *SPE* (MJ/kg) = C_0 + C_1 / DR_a (kg/min).

Set of data	C_0 (MJ/kg)	[95% confidence bounds]	C_1 (MJ/min)	[95% confidence bounds]	R^2
Components printed in ABS	4.18	[0.00, 9.64]	$2.92 \cdot 10^{-2}$	[$2.81 \cdot 10^{-2}$, $3.04 \cdot 10^{-2}$]	0.99
Components printed in PC-ABS	5.07	[0.69, 9.44]	$3.04 \cdot 10^{-2}$	[$2.94 \cdot 10^{-2}$, $3.13 \cdot 10^{-2}$]	0.99
All the printed components	4.81	[0.90, 8.73]	$2.97 \cdot 10^{-2}$	[$2.89 \cdot 10^{-2}$, $3.06 \cdot 10^{-2}$]	0.99

The C_0 and C_1 coefficients are listed in Table 6, while considering different sets of data. C_0 (in MJ/kg) is a constant not related with the deposition time, and is representative of a fixed Specific Energy Consumption that has to be included independently from the value of the DR_a. The energy consumption due to the C_0 term increases linearly when the mass to be deposited increases. C_1 (in MJ/min) quantifies the constant power rate due to the energy consumption of equipment such as the heating system of the build chamber, extruders' heaters, electronic control, fan, et cetera. Therefore, C_1 is mainly linked to the architecture of the machine. Moreover, despite the small numerical differences due to the printed materials, Equation 2 can be applied to characterize the FDM machine, since the R^2 value of the model regarding all the experimental data is higher than 0.99. Overall, the total electric energy consumption of the FDM process (E^{FDM}, in MJ) can also be computed according to Equation 3,

$$E^{\text{FDM}} = E_{\text{constant}} + \text{SPE} \cdot m_{\text{tot}} = E_{\text{constant}} + \left(C_0 + \frac{C_1}{\text{DR}_a} \right) \cdot m_{\text{tot}} \tag{3}$$

where m_{tot} (in kg) is the total mass of material (for the component, support structures and purge part) to be deposited. It is worth remarking that the same modelling approach can be used while extending the analysis to the entire FDM unit-process (i.e., including both the printing and the non-printing phases), as shown in Figure 13.
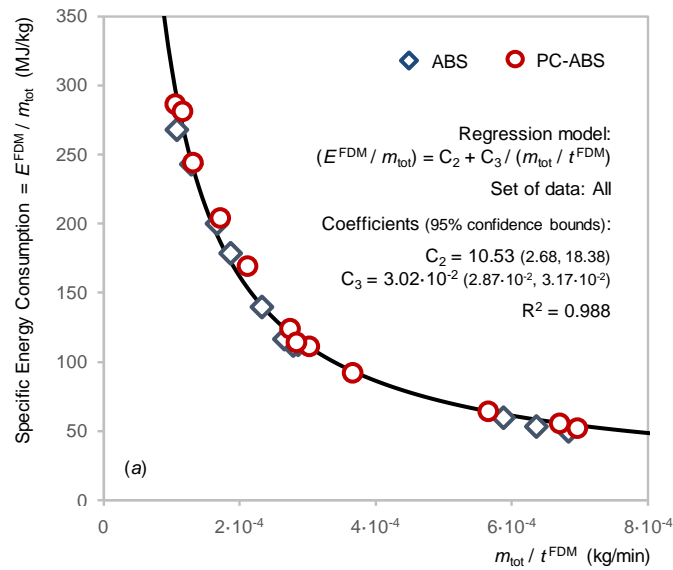

Figure 13. An example of the application of the model to the entire FDM process (including productive and non-productive times).

4.4. Model validation

In order to validate the above-proposed equations, the same amounts of material characterizing the component 'A' (i.e., the basket) were deposited by producing, in the same job, two cubes made of PC-ABS and QSR having dimensions of 29.2 x 29.2 x 29.2 mm^3 and 48.9 x 48.9 x 48.9 mm^3, respectively. The total deposited mass (m_{tot}, including the purge part) was 149.5 g. The process time and the energy consumption were measured, and the results are summarized in Figure 14. The printing time (t_4) was 301 min (5.01 h), coherently with the expected time of 311 min obtained by means of a simulation preliminarily performed by the GrabCAD Print software. Therefore, the average Deposition Rate (DR$_a$ = m_{tot} / t_4) was computed to be 4.97·10^{-4} kg/min. The Specific Printing Energy (SPE) of the deposition phase can be quantified by using Equation 2. If the average coefficients C_0 and C_1 for PC-ABS (equal to 5.07 MJ/kg and 3.04·10^{-2} MJ/min, respectively) are applied, the SPE is 66.2 MJ/kg and the resultant electric energy consumption for the printing phase (E_4) is 9.90 MJ. The difference between the so-computed value and the measured value of 9.47 MJ (2.63 kWh) is below the 5% of the total. Moreover, E_4 can also be obtained by multiplying the printing time t_4 and the 'a' coefficient of the linear regression (according to Equation 1). When 'a' is set to 3.03·10^{-2} MJ/min, the computed value for E_4 is 9.12 MJ, and the model-to-experimental difference is below 4% of the total. Satisfactorily comparable results can be achieved by using the 'a', 'C$_0$' and 'C$_1$' coefficients regarding the entire set of the experimental data, regardless of the kind of component material.
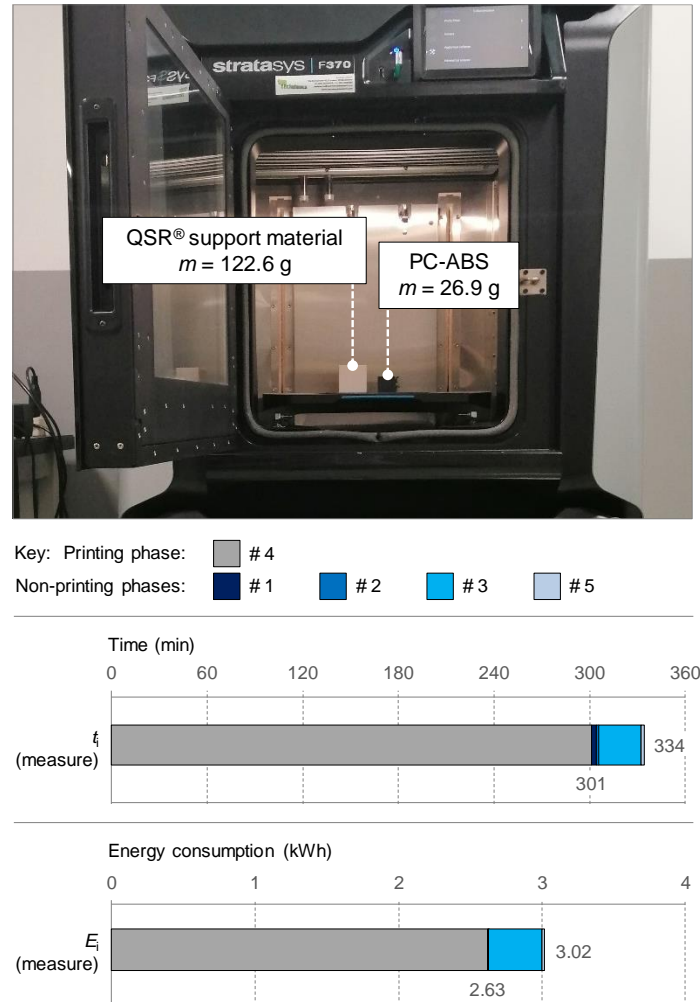
Figure 14. Experimental test for model validation.

In addition, the printing time for the component 'A' was 23.4 h. The time for printing the same mass of materials in the simpler shape chosen to validate the model was reduced to approximately one fifth. Also, the energy consumption was

proportionally lower. This experimental evidence confirms that the complexity in the deposition path affects directly the average Deposition Rate, as above explained, as well as the process outcomes.

5. Conclusions

An experimental campaign aimed to identify the effects of the main FDM parameters on the process time and energy consumption was carried out in this research. Components characterized by different geometrical complexities and requiring variable volumes of the support structures were printed in ABS and PC-ABS by means of a Stratasys F370 FDM machine. The layer thickness and the infill strategy were included among the input variables. The main process phases were identified while considering the complete unit-process. The analysis of the results showed that the contribution due to the non-printing phases (i.e., during the switch-on, idling, heating and calibration operational modes) on the total process time and energy consumption can be modelled as a constant. As far as the printing phase is concerned, a linear correlation between build time and energy demand for printing was highlighted. Moreover, negligible differences were noticed when the extruder prints the material of which the component is made (either ABS or PC-ABS) or the QSR material for the support structures. Therefore, it was possible to propose an inverse model correlating the Specific Printing Energy and the average Deposition Rate (which was defined, for the purpose of this research, as the ratio between the total mass of deposited materials and the build time). The average Deposition Rate was seen as a holistic measure of the job complexity and consequently of the deposition path, which in turn was proved to depend on the chosen process parameters, the material to be deposited and the component shape. The coefficients of the empirical models were computed by means of regression analyses for each printed material of the component (ABS or PC-ABS). Moreover, since the differences among the numerical values are small, a model for the entire FDM machine was suggested.

The proposed models can be used to predict the energy consumption of the complete process, being known the mass of all the deposited materials (to make the component, the support structures, and the purge part) and the build time. Such data can be easily obtained a priori from simulations performed by means of the software supplied with the machine. With reference to the existing literature, the present paper contributes to a more accurate description of the correlation between the FDM average Deposition Rate and the Specific Energy Consumption, and aims to foster the debate concerning the sustainability of AM processes [30, and references therein]. One of the strategies towards the energy consumption reduction could be the increase in the deposition speed and the optimization of the extruders' path per each layer, which in some cases are difficult to be controlled by the operator (particularly for closed-architecture machines). Finally, it is interesting to remark the analogies between the results achieved in this research and the unit-process model for machining firstly introduced by Kara and Li [15,16], who proposed the same inverse law to correlate the Specific Energy Consumption and the material removal rate. The same model was also applied to Friction Stir Extrusion [31] and injection molding processes [32]. These empirical models, mainly dependent on the machine architecture as well as the process control, appear to be striking successful for all the manufacturing processes in which the constant power requirement of the machine equipment (such as the heating systems for FDM) dominates the total energy consumption.

References

[1] Calignano F, Manfredi D, Ambrosio EP, Biamino S, Lombardi M, Atzeni E, Salmi, A, Minetola, P, Iuliano, L, Fino, P. Overview on Additive Manufacturing Technologies. Proceedings of the IEEE 2017; 105:593-612. DOI: 10.1109/JPROC.2016.2625098.

[2] Gibson I, Goenka G, Narasimhan R, Bhat N. Design rules for additive manufacture. 21st Annual International Solid Freeform Fabrication Symposium - An Additive Manufacturing Conference, SFF 2010; 705-716. Code: 104346.

[3] Salmi A, Calignano F, Galati M, Atzeni E. An integrated design methodology for components produced by laser powder bed fusion (L-PBF) process. Virtual and Physical Prototyping 2018; 191-202. DOI: 10.1080/17452759.2018.1442229.

[4] Atzeni E, Iuliano L, Marchiandi G, Minetola P, Salmi A, Bassoli E, Denti L, Gatto A. Additive manufacturing as a cost-effective way to produce metal parts. High Value Manufacturing, CRC Press 2013; 3-8. DOI: 10.1201/b15961-3.

[5] Singh S, Ramakrishna S, Singh R. Material issues in additive manufacturing: A review. Journal of Manufacturing Processes 2017; 25:185-200. DOI: 10.1016/j.jmapro.2016.11.006.

[6] Hopkinson, N, Dickens P. Analysis of rapid manufacturing - using layer manufacturing processes for production. Proceedings of the Institution of Mechanical Engineers, Part C: Journal of Mechanical Engineering Science 2003; 217(1):31-40. DOI: 10.1243/095440603762554596.

[7] Ingole DS, Kuthe AM, Thakare S., Talankar AS. Rapid prototyping – a technology transfer approach for development of rapid tooling. Rapid Prototyping Journal 2011; 15(4):280–290. DOI: 10.1108/13552540910979794.

[8] Dawoud D, Taha I, Ebeid SJ. Mechanical behaviour of ABS: An experimental study using FDM and injection moulding techniques. Journal of Manufacturing Processes 2016; 21:39-45. DOI: 10.1016/j.jmapro.2015.11.002.

[9] Sezer HK, Eren O. FDM 3D printing of MWCNT re-inforced ABS nano-composite parts with enhanced mechanical and electrical properties. Journal of Manufacturing Processes 2019; 37:339-347. DOI: 10.1016/j.jmapro.2018.12.004.

[10] Geng P, Zhao J, Wu W, Ye W, Wang Y, Wang S, Zhang, S. Effects of extrusion speed and printing speed on the 3D printing stability of extruded PEEK filament. Journal of Manufacturing Processes 2019; 37:266-73. DOI: 10.1016/j.jmapro.2018.11.023.

[11] Kellens K, Mertens R, Paraskevas D, Dewulf W, Duflou J. Environmental Impact of Additive Manufacturing Processes: Does AM contribute to a more sustainable way of part manufacturing? Procedia CIRP 2017; 61:582-587. DOI: 10.1016/j.procir.2016.11.153.

[12] Yoon H, Lee J, Kim H, Kim M, Kim E, Shin, Y-J, Chu, W-S, Ahn, S-H. A comparison of energy consumption in bulk forming, subtractive, and additive processes: Review and case study. International Journal of Precision Engineering and Manufacturing - Green Technology 2014; 1:261-279. DOI: 10.1007/s40684-014-0033-0.

[13] Kellens K, Baumers M, Gutowski TG, Flanagan W, Lifset R, Duflou JR. Environmental Dimensions of Additive Manufacturing. Mapping Application Domains and Their Environmental Implications. Journal of Industrial Ecology 2017; 21:S49-68. DOI: 10.1111/jiec.12629.

[14] Junk S, Côté S. A practical approach to comparing energy effectiveness of rapid prototyping technologies. Proceedings of AEPR'12, 17th European Forum on Rapid Prototyping and Manufacturing 2012.

[15] Kara S, Li W. Unit process energy consumption models for material removal processes. CIRP Annals - Manufacturing Technology 2011; 60(1):37-40. DOI: 10.1016/j.cirp.2011.03.018.

[16] Li W, Kara S. An empirical model for predicting energy consumption of manufacturing processes: A case of turning process. Proceedings of the Institution of Mechanical Engineers, Part B: Journal of Engineering Manufacture 2011; 225(9):1636-1646. DOI: 10.1177/2041297511398541.

[17] Luo Y, Ji Z, Leu MC. Environmental performance analysis of solid freeform fabrication processes. IEEE International Symposium on Electronics and the Environment 1999; 1-6. CODEN: 85OPA.

[18] Le Bourhis F, Kerbrat O, Hascoet J, Mognol P. Sustainable manufacturing: Evaluation and modeling of environmental impacts in additive manufacturing. International Journal of Advanced Manufacturing Technology 2013; 69(9-12):1927-1939. DOI: 10.1007/s00170-013-5151-2.

[19] Yosofi M, Kerbrat O, Mognol P. Energy and material flow modelling of additive manufacturing processes. Virtual and Physical Prototyping 2018; 13(2):83-96. DOI: 10.1080/17452759.2017.1418900.

[20] Mognol P, Lepicart D, Perry N. Rapid prototyping: energy and environment in the spotlight. Rapid Prototyping Journal 2006; 12(1):26-34. DOI: 10.1108/13552540610637246.

[21] Baumers M, Tuck C, Bourell DL, Sreenivasan R, Hague R. Sustainability of additive manufacturing: measuring the energy consumption of the laser sintering process. Proceedings of the Institution of Mechanical Engineers, Part B: Journal of Engineering Manufacture 2011; 225(12):2228-2239. DOI: 10.1177/0954405411406044.

[22] Baumers M, Tuck C, Wildman R, Ashcroft I, Hague R. Energy inputs to additive manufacturing: does capacity utilization matter? 22nd Annual International Solid Freeform Fabrication Symposium - An Additive Manufacturing Conference, SFF 2011; 30-40. Code: 104347.

[23] Huang R, Riddle M, Graziano D, Warren J, Das S, Nimbalkar S, Cresko, J, Masanet, E. Energy and emissions saving potential of additive manufacturing: the case of lightweight aircraft components. Journal of Cleaner Production 2016; 135:1559-1570. DOI: 10.1016/j.jclepro.2015.04.109.

[24] Balogun VA, Kirkwood N, Mativenga PT. Energy consumption and carbon footprint analysis of Fused Deposition Modelling: A case study of RP Stratasys Dimension SST FDM. International Journal of Scientific & Engineering Research 2015; 6(8).

[25] Yosofi M, Kerbrat O, Mognol P. Additive manufacturing processes from an environmental point of view: a new methodology for combining technical, economic, and environmental predictive models. International Journal of Advanced Manufacturing Technology 2019; 102(9-12):4073-4085. DOI: 10.1007/s00170-019-03446-2.

[26] Stratasys ABSplus-P430 Datasheet.
www.stratasys.com/-/media/files/material-spec-sheets/mss_fdm_absplusp430_1117a.pdf (Accessed on May 14, 2020).

[27] Stratasys PC-ABS Datasheet.
www.stratasys.com/-/media/files/material-spec-sheets/mss_fdm_pcabs_1217a.pdf (Accessed on May 14, 2020).

[28] Duflou JR, Sutherland JW, Dornfeld D, Herrmann C, Jeswiet J, Kara S, et al. Towards energy and resource efficient manufacturing: A processes and systems approach. CIRP Annals - Manufacturing Technology 2012; 61(2):587-609. DOI: 10.1016/j.cirp.2012.05.002.

[29] Guo Y, Duflou JR, Qian J, Tang H, Lauwers B. An operation-mode based simulation approach to enhance the energy conservation of machine tools. Journal of Cleaner Production 2015; 101, 5398: 348-359. DOI: 10.1016/j.jclepro.2015.03.097.

[30] Minetola P, Priarone PC, Ingarao G. Sustainability for 3DP Operations. In: Managing 3D Printing - Operations Management for Additive Manufacturing (D. Eyers ed.), 2020: 97-126, Palgrave Macmillan, Cham, ISBN: 978-3-030-23322-8. DOI: 10.1007/978-3-030-23323-5_7.

[31] Baffari D, Reynolds AP, Masnata A, Fratini L, Ingarao G. Friction stir extrusion to recycle aluminum alloys scraps: Energy efficiency characterization. Journal of Manufacturing Processes 2019; 43:63-69. DOI: 10.1016/j.jmapro.2019.03.049.

[32] Thiriez A. An environmental analysis of injection molding. Massachusetts Institute of Technology, 2006. http://hdl.handle.net/1721.1/35646 (Accessed on September 13, 2019).